Journal of Geodesy (1998) 72: 442–459

Journal of Geodesy

© Springer-Verlag 1998

Study of a wide-angle laser ranging system for relative positioning of ground-based benchmarks with millimeter accuracy

O. Bock[1,2], M. Kasser[1,2], C. Thom[2], J. Pelon[3]

[1]Ecole Supérieure des Géomètres et Topographes-Conservatoire National des Arts et Métiers, Le Mans, France
[2]Lab. d'Optoélectronique et de Microinformatique-Institut Géographique National, 2 av. Pasteur, F-94165 Saint Mandé Cedex, France
Tel: +33 1 43 98 83 92; fax: + 33 1 43 98 85 81; e-mail: Olivier.Bock@ign.fr
[3]Service d'Aéronomie-Centre National de la Recherche Scientifique, Université Pierre et Marie Curie, Paris, France

Received: 19 June 1997 / Accepted: 17 February 1998

Abstract. A wide-angle airborne laser ranging system (WA-ALRS) is developed at the Institut Géographique National (IGN), France, with the aim of providing a new geodesy technique devoted to large (100 km^2) networks with a high density (1 km^{-2}) of benchmarks. The main objective is to achieve a 1-mm accuracy in relative vertical coordinates from aircraft measurements lasting a few hours. This paper reviews the methodology and analyzes the first experimental data achieved from a specific ground-based experiment. The accuracy in relative coordinate estimates is studied with the help of numerical simulations. It is shown that strong accuracy limitations arise with a small laser beam divergence combined with short range measurements when relatively few simultaneous range data are produced. The accuracy is of a few cm in transverse coordinates and a few mm in radial coordinates. The results from ground-based experimental data are fairly compatible with these predictions. The use of a model for systematic errors in the vehicle trajectory is shown to be necessary to achieve such a high accuracy. This work yields the first complete validation of modelization and methodology of this technique. An accuracy better than 1 mm and a few mm in vertical and horizontal coordinates, respectively, is predicted for aircraft experiments.

Key words. Laser ranging · Airborne · Multilateration

1 Introduction

1.1 Instrumental needs for monitoring geophysical processes

High-precision geodesy becomes more and more involved with the study of local geophysical processes, among which are tectonic motions, landslides resulting from geological instabilities, and land subsidence stemming from solid extraction or fluid withdrawal. Volcano monitoring and earthquake prediction programs also become numerous. Most of these geodynamic phenomena produce deformations scaling from less than 1 mm/year to above 10 cm/day. It is generally recognized that vertical deformations always accompany horizontal deformations, though of much smaller amplitude. Our interests particularly concern monitoring vertical deformations, and accordingly we concentrate only on these. Ruegg and Kasser (1990) have reported 1–10-cm uplifts during a rifting process lasting a few days. Rates of 1 mm/year to 1 cm/year were found for plate motion (Tapley et al. 1985; Christodoulidis et al. 1985; Smith et al. 1990). Massonnet et al. (1995) reported 1–10-cm deformations for Mount Etna. Land subsidence due to fluid withdrawal is observed in a wide range, from 1 mm/year to 10 cm/year (e.g., Heywood 1995). The main interest of accurate measurements of subsidence above hydrocarbon fields is for solving inverse problems, i.e., estimating the spatial extension of reservoirs. This would increase the effectiveness of gas-field production (Bouteca et al. 1990; Fourmaintraux et al. 1994). Similar efforts are made in the field of general geodynamics (Dingwen 1989).

From the foregoing considerations it is evident that a geodesy technique is needed for surveying dense networks, which would be rapid and highly accurate. Specifically, networks of ~100 km^2 with ~1-km^{-2} densities will be considered for which the accuracy in relative vertical coordinate estimates should be below the 1-mm level from a single session which would last less than 1 day.

1.2 Current instrumental solutions

Geodynamic deformations are commonly monitored by measuring changes in coordinates or in baselines of a network of ground-based benchmarks. Historically, high-precision leveling has been the only technique

Correspondence to: Olivier Bock[2]

achieving millimeter accuracy in relative heights of benchmarks separated by a few kilometers. However, this technique requires painstaking and time-consuming efforts, especially for large networks. During the last two decades several alternatives and most modern (e.g., spatial) techniques have been developed: VLBI (Very Long Baseline Interferometry), SLR (Satellite Laser Ranging), DORIS (Détermination d'Orbites par Radiopositionnement Intégré au Satellite), GPS (Global Positioning System), GLRS (Geoscience Laser Ranging System), and more recently In-SAR (Interferometric-Synthetic Aperture Radar). In these techniques station coordinates are adjusted from distance and/or phase measurements. The main error source is correction for atmospheric path-delay (PD). Hence, one has to distinguish between two technologies, whether radio or optical wavelengths are used. We shall briefly review the accuracy achievable with the aforementioned techniques and their capabilities for surveying dense networks such as defined.

Let us first consider radiowaves. For such wavelengths PD has basically two origins: charged particles in the ionosphere and atmospheric gases in the troposphere. Since the ionosphere is dispersive, the effect of the former is removed within 0.3 mm with dual-frequency measurements (Lundqvist 1984). On the other hand, the effect of the troposphere must be corrected a priori with the help of meteorological data. Whereas the contribution from dry air is easily corrected from surface pressure measurements, contribution from water vapor is much more difficult to correct since this constituent is highly variable. The ranging accuracy is then limited to the 1-cm level (Davis et al. 1985). As a consequence, the precision in vertical coordinate estimates is limited to this level. Different techniques have been experienced either for compensating the effect of water vapor, such as least-squares adjustment and Kalman filtering, or for estimating the actual water vapor content with water vapor radiometers (WVR). Glaus et al. (1995) and Dodson et al. (1996) report a repeatability in vertical coordinates of 5 and 9 mm, respectively, from GPS measurements of baselines smaller than 200 km. Ware et al. (1993) report 2.6-mm precision for 50-km baselines. They show that pointed WVR yields the best results with respect to other techniques, namely zenith WVR. However, for small baselines, of order $\sim$1 km, most of the PD uncertainties are eliminated in coordinate differences. For such cases, absolute PD corrections are not required. Genrich and Bock (1992) report 4-mm repeatability in the vertical component from kinematic GPS surveys, with 30-min occupation times and favorable satellite geometry. Fourmaintraux et al. (1994) report down to 3-mm repeatability from GPS measurements averaged over 3 days in a small network over a flat area. Herring (1992) reports 2.3-mm repeatability from VLBI phase delay measurements of 1.24-km baseline. Regarding DORIS and In-SAR, the problem is quite different. Presently, the former technique is restricted to large baselines. However, relatively high accuracies have been achieved. Willis (1996) reports 2.5-cm precision for a 1-week DORIS session. The accuracy of In-SAR seems not yet clearly assessed. However, an instrumental resolution is estimated of about 1 cm in radial coordinates from a single interferogram (Massonnet et al. 1995). Additionally to atmospheric effects, this technique also suffers from seasonal soil variations which may limit its accuracy to a few centimeters.

Optical signals are not affected by the electron content of the atmosphere. Hence, atmospheric PD limitations arise only in the troposphere. However, the sensitivity of optical signals to water vapor is much smaller (by a factor of 100) than for radio signals. Absolute zenith PD corrections are predicted within a few millimeters from surface meteorological measurements (Marini and Murray 1973). This uncertainty compares with the instrumental precision of modern SLR systems (Degnan 1993). Regarding spaceborne laser ranging techniques, such as GLRS, only numerical simulations have been reported to date. Khan et al. (1980) have predicted a relative vertical repeatability between 4 mm and 4 cm, for baselines between 50 and 500 km, with 1000 measurements per cube-corner retroreflector (CCR). They accounted for various bias and noise sources in range measurements: system noise and bias, atmospheric delay correction, atmospheric drag, cloud cover, earth gravity field, and solar radiation pressure. Cohen et al. (1987) assessed the accuracy in baselines and relative coordinates by means of a covariance error analysis. They found an uncertainty (from noise and bias) in relative vertical coordinates between 2 mm and 2 cm, with baselines between 50 and 500 km and about 200 measurements per CCR. They accounted for the same error sources (bias and noise) as reported by Kahn et al. (1980) except for the system bias, though one is expected in practice. They clearly demonstrate that GLRS techniques should achieve a relative height determination of CCRs at the subcentimeter level with short baselines. However, we emphasize that both approaches neglected biases stemming from local meteorological effects in the convective boundary layer. Furthermore, the instrumental uncertainty was assumed to be 1 cm for all measurements, thus neglecting the angular dependence of the link budget and atmospheric induced scintillation.

Of the aforementioned techniques, only GPS and GLRS yield possibilities for regional or local geodesy in small, dense networks. However, in the case of GPS, an accuracy of a few mm in the vertical, with short survey durations, would require one receiver at each station, which is quite inconvenient. Hence, GLRS-like systems are preferred. Those systems use either true simultaneous- or rapid sequential-laser range measurements. From such measurements, both the orbit (or trajectory in the case of an aircraft) of the instrumented platform and the CCR coordinates are adjusted with mm to cm accuracy. Several attempts have been made in the past to develop such systems (Kahn et al. 1980; Cohen et al. 1987; Lutz et al. 1982; Khan et al. 1982). But the use of multiple-beam and/or servo-controlled pointing systems made them rather complicated, and they were finally abandoned. Nevertheless, we find that simultaneously measuring several distances is really advantageous since

it strongly reduces the accuracy required on the a priori platform trajectory and atmospheric PD correction. The wide-angle airborne laser ranging system (WA-ALRS) developed at IGN is based on this principle but different instrumental and signal processing approaches are used for achieving the simultaneous range measurements (Kasser 1991; Bock et al. 1995).

1.3 Outline of the paper

The future WA-ALRS will be an airborne instrument providing simultaneous pseudo-range (PR) measurements to a network of ground-based CCRs. Its objective is to provide relative-position estimates with millimeter accuracy in the vertical coordinate for configurations as specified in Sect. 1.1. Up to now, several steps have been validated in the study of this technique. Bock et al. (1995) have developed and characterized a prototype instrument for multiple-range measurements, which is briefly described in Sect. 2 along with the principle of the future aircraft applications. In Sect. 3 we summarize the results from a careful study of instrumental error sources, atmospheric effects, and measurement scenario conducted by Bock (1996). The mathematical formulation for the inverse problem (multilateration) is presented in Sect. 4. The forward model accounts for the specificity of the ground-based experiment and for systematic errors in the a priori vehicle trajectory, as obtained from differential-GPS (DGPS) trajectography measurements. A modified least-squares adjustment is used for solving the inverse problem. In Sect. 5, numerical simulations are used for studying the effects of different experimental parameters on positioning accuracy in a specific ground-based configuration. Among these, unresolvable parameters (such as vertical coordinates owing to horizontal measurements and arbitrarily-fixed CCRs), laser beam divergence, offsets and drifts in vehicle trajectory, and pseudo-range offsets (PROs) are considered. In Sect. 6 the simulation results are compared to experimental results reported by Bock et al. (1997). It is shown that both agree well and that the specific configuration imposes a limit of 1–2 mm in radial coordinates.

The work presented in this paper is thus composed of a review on the multilateration technique developed at IGN (Sects. 2, 3 and 4) and of an analysis of the accuracy achievable in a specific ground-based configuration in which an experiment has been conducted (Sects. 5 and 6). The results are summarized and discussed in Sect. 7.

2 Principle of the WA-ALRS

2.1 Aerial multilateration

In our system multilateration is achieved with a wide-angle (divergent) laser beam transmitted from an airborne platform toward a network of ground-based CCRs (cf. Fig. 1). For any transmitted laser pulse, CCRs produce simultaneously in return a set of echoes. Hence, simultaneous ranges can be measured between the instantaneous location of the airborne platform and the CCRs within the laser beam pattern. They produce strong geometrical constraints between CCR coordinates, but also on instantaneous relative locations of the airborne platform. Hence, both CCR coordinates and vehicle locations, at each laser-shot (LS), can be estimated with a least-squares adjustment. Since the laser beam pattern is of finite extent (~5 km in diameter), only a part of the network is seen. With a proper aircraft flight-path, constraints, are produced

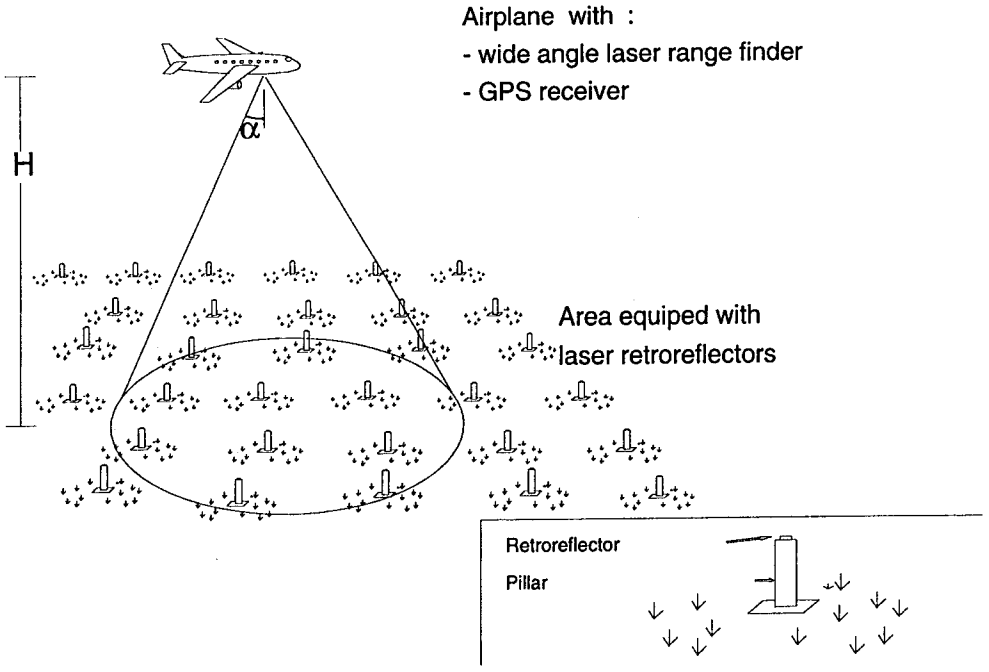

Fig. 1. View of a typical aircraft experiment over a ground-based retroreflector network

between all the CCRs of the network. Hence, the estimated CCR coordinates are relative coordinates with respect to fixed CCRs (usually on the border of the network).

A priori aircraft and CCR locations, which are required for the adjustment procedure (see Sect. 4), are easily achieved with DGPS techniques. Aircraft trajectography from DGPS measurements is commonly used for aerial triangulation in photogrammetry. With single-frequency receivers, the positioning accuracy is of ~ 50 cm. Rapid-static DGPS can be used for achieving a priori CCR locations. With a few minutes of observation at each station, an accuracy of a few cm is easily achieved. Note that the survey of the CCR network has only to be performed once, before the first aerial survey; subsequent surveys can simply use the results from previous surveys as a priori data.

2.2 Instrument

The originality of this system lies both in the use of a widely divergent laser beam and a slow detector. These solutions simplify considerably the apparatus, with respect to the multiple-beam ranging system proposed by Khan et al. (1982). However, proper signal processing is required in order to identify which CCRs are measured for any transmitted laser pulse (see Sect. 2.3).

A block diagram of the wide-angle laser ranging system is illustrated in Fig. 2. A mode-locked Nd:YAG laser transmits a 100-ps pulse (full width at half maximum: FWHM) of about 100 mJ, with a repetition frequency of 10 Hz. In the future system, the wide-angle beam will be produced by a diverging lens. However, in the ground-based experiment considered below a ground glass plate was used, though it produced speckle patterns which increased irradiance fluctuations. In the present system, laser echoes are detected by a large area (1 cm^2) PIN photodiode (EG&G, YAG 444), and magnified by an in-house transimpedance amplifier (3000 V/A gain, 50-MHz bandwidth, 10 $nV/Hz^{-1/2}$ noise). Waveforms are sampled by a digital osilloscope (LeCroy 7200, 1 Gs/s, 500-MHz bandwidth), and transferred in real time to a portable PC (Fieldworks 7500). However, only a small window of time, centered on the times of arrival of the echoes, is recorded. Hence, only those times of arrival can be estimated since the corresponding time of emission is not recorded. The rather long transit time (~ 6 ns) of the photodiode increases the duration of measured pulses to ~ 13 ns (FWHM) with, however, a ~ 4-ns leading edge at half-intensity. The measured pulse shapes are thus roughly equal to the impulse response of the detection stage. Therefore, a matched-filter-type detection appears natural for estimating the times of arrival (see Sect. 2.3.2).

The current system achieves an optical link budget (received to transmitted power ratio) of order $\gamma \sim 10^{-11}$ on the beam axis, with a laser beam divergence of $\alpha = 20°$ (half-angle at $1/e^2$ intensity) and a distance of order 1 km. The corresponding signal-to-noise ratio is of SNR ~ 100. Hence, for short ranges, the single-shot accuracy in PR measurements is between a few mm and few cm (see the following). Future aircraft experiments at an altitude of $h = 10$ km would yield optical link budgets of order $\gamma \sim 10^{-14}$. The performance of the current system would thus not be sufficient to achieve cm-precision PR measurements. The system is presently optimized to meet the requirement of SNR = 50 in such conditions.

2.3 Data processing

The data processing sequence can be divided into four steps as described in the following.

2.3.1 A priori data processing. Once a priori CCR coordinates are known (e.g., results from a previous survey), and the aircraft trajectory is calculated (from DGPS data measurements), a priori ranges are estimated between all CCRs and aircraft. Therefore, the measured aircraft trajectory is interpolated for each measurement epoch, i.e., for each LS with a 0.1-s interval. The accuracy of a priori ranges is thus of order 1 m, which is sufficient for the following signal processing.

2.3.2 Signal processing. The measured signal (see Fig. 3) is a record of digitized laser echoes. These are detected, identified, and timed (or ranged). Therefore, the following procedure is applied to each and every record.

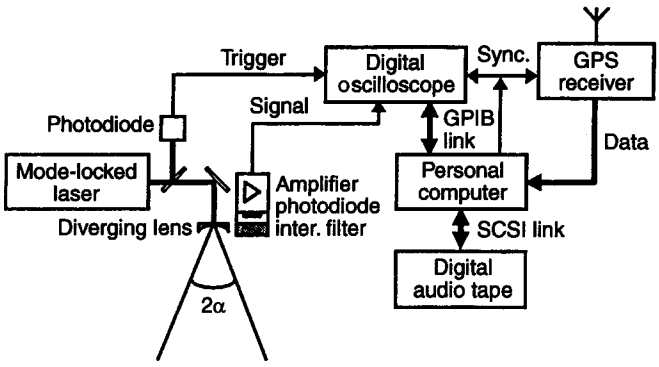

Fig. 2. Block diagram of the wide-angle laser ranging instrument. An additional ground-based GPS receiver is required for performing DGPS trajectography measurements

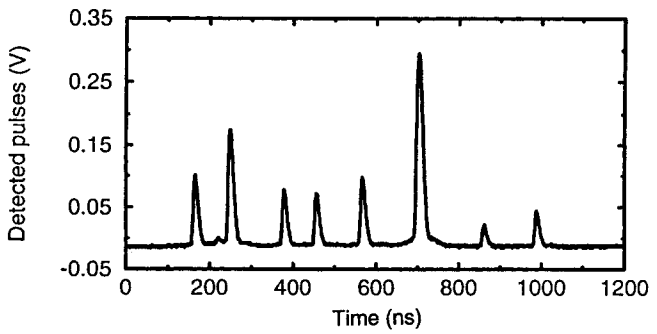

Fig. 3. Typical signal (arbitrary origin of times) when distances to CCRs are between 500 m and 1 km (from Combs-la-Ville experiment, 1995)

1. The time of emission is roughly estimated, which is common to all echoes of a given record. Therefore the measured signal is cross-correlated with a Dirac comb composed of pulses located at the a priori times of arrival of the expected echoes. The latter times are computed from a priori ranges calculated in the first step. The accuracy in estimates of time of emission is of about the sampling interval of the digital signal, i.e., ~1 ns (15 cm). As a further result of that cross-correlation, echoes are detected with a threshold in SNR of 3, and CCRs are identified.

2. Accurate times of arrival for all echoes of any record are estimated conjointly with a least-squares adjustment. The method is a kind of deconvolution of the measured signal with respect to the impulse response of the detection stage. This estimation technique is actually equivalent to a cross-correlation between the measured signal and the impulse response (Bock 1996). It is thus optimal for the case of a signal with additive white noise (matched filter). Its performance has been assessed both theoretically and experimentally (see next section; Bock et al. 1997).

3. PRs are calculated from the times of arrival after correction for instrumental biases and atmospheric PD. In fact, only PRs are achieved, as in GPS measurements, since the time of emission is not known precisely. Consequently, a common offset, referred to as the PRO, is present in PRs achieved from a given record. When systematic errors are properly corrected, PROs fluctuate from shot-to-shot with peak-to-peak values of ±0.5 ns (±7.5 cm).

2.3.3 Outlier detection. Before PR measurements are used in the adjustment procedure, outliers must be carefully detected. This is a major requirement since the adjustment procedure (see Sect. 4) is implemented as a least-squares method. With our wide-angle laser beam, pulse superimposition stemming from coincident echoes is a major source of systematic errors. Such superimposition produces distortions in the pulse shapes of echoes which lead to dramatic biases in estimates of time of arrival. For instance, two echoes with a typical pulsewidth of 13 ns (1.95 m) FWHM begin to overlap and distort each other when their separation in time is below ~30 ns. The latter value is thus used as a threshold for sorting detected echoes on the basis of a priori ranges. However, when relatively few echoes are measured simultaneously, the PRO estimates might be strongly corrupted. For such cases, CCR misidentifications are likely. This is another source for outliers. A simple method for detecting such errors consists in putting a threshold (about a few centimeters) on the standard deviation in a priori residuals (the residual is the difference between a priori range and estimated PR), for every record. Note that a priori residuals contain systematic errors owing to PROs. These errors are removed when considering the standard deviation in residuals which is, by definition, corrected for the mean value.

2.3.4 Vehicle and CCR coordinates adjustment. To give some insight into the data volume to be handled in the adjustment procedure, let us consider a network of $N_{CCR} = 100$ and a typical aircraft experiment yielding $N_{LS} = 2 \times 10^4$ (Bock 1996). The number of unknowns is of $3 \times N_{CCR}$ (three coordinates) + $4 \times N_{LS}$ (three coordinates + 1 PRO), i.e., of order $4 \times N_{LS} = 8 \times 10^4$. With a typical number of PR measurements, $N_{Meas} = 3 \times 10^5$, the problem is strongly overdetermined (Bock 1996). Hence, a substantial uncertainty reduction is possible. Namely, with an uniform (bias-free) ranging accuracy of order $\sigma_\rho \sim 5$ cm, the precision in radial coordinates would be of order $\sigma_\rho / N_{Meas/CCR}{}^{1/2} \sim 1$ mm, where $N_{Meas/CCR} = 3 \times 10^3$ is the average number of (independent) measurements per CCR. The latter number is adapted to the experiment configuration through N_{LS}, i.e., duration of the flight path. Obviously, the lower limit for N_{Meas} is equal to the number of unknowns.

The number of measurements per laser shot (LS), $N_{Meas/LS}$, is a further parameter conditioning the positioning accuracy. Actually, it determines to the first order the accuracy in estimates of vehicle coordinates which in return may influence the accuracy in estimates of CCR coordinates. Obviously, this number has to be strictly greater than the number of unknowns related to each and every LS, i.e., $N_{Meas/LS} > 4$ in the case of an aircraft experiment. The more distances measured simultaneously, the stronger the constraints on relative vehicle coordinates. This number depends on a combination of laser beam divergence, aircraft altitude, system SNR, and CCR density. With $\alpha = 20°, h = 10$ km, SNR = 50 and a 1-km^{-2} CCR density, $N_{Meas/LS} \sim 20$ (Bock 1996).

Note that such a geometrical configuration of PR measurements is favourable to a higher accuracy in the vertical than in the horizontal coordinates. Reducing α would increase the accuracy in the vertical but also simultaneously decrease the accuracy in the horizontal. Hence, the uncertainty in vehicle coordinates might become critical, i.e., $N_{Meas/LS}$ would approach its critical value. This effect is similar to GPS satellite sky distribution reported by Santerre (1991).

3 Error sources

3.1 Atmosphere

In the introduction, PD owing to atmospheric refraction has been considered as the ultimate error source in range measurements through the atmosphere (both radio and optical). However, with respect to the spatial geodesy techniques discussed, our system is much less sensitive to PD. Actually, those errors which are repetitive between experiments vanish when differential coordinates are considered. A rough correction of the overall PD is thus sufficient, which would be achieved from the pressure difference between the aircraft and CCRs. The pressure at CCRs would be estimated from a few surface meteorological measurements only, since it is not realistic to put as many meteorological stations as CCRs. Note that the mean PD would also be compensated by the adjustment of PROs. Actually, only

differential PDs, i.e., between CCRs, need to be corrected since relative ranges are measured. Consequently, with our system the ultimate error source in PR measurements is with horizontal gradients or deviations in temperature profiles between CCRs, i.e., mainly within the boundary layer. A first assessment for such deviations, assuming a static atmosphere on the timescale of the experiment, has been made (Bock 1996). It has been shown that a 1 °C deviation constant over through a 1-km boundary layer would produce biases of order 1 mm. Such deviations are likely over inhomogeneous terrain. However, for the ground-based experiment on which we will focus in the following, such systematic errors should be negligible. Additionally, moderate turbulence would produce PD fluctuations with a standard deviation of 1 mm, which is negligible compared with instrumental errors.

Additionally to deviations in PD, scintillation owing to atmospheric turbulence might influence the positioning accuracy. The effect of scintillation is basically a random modulation of the return intensity which might reduce the geometrical constraints produced by the PR measurements. The probability that the intensities of the measured echoes are at least equal to those of the scintillation-free case is small. However, the net effect is not necessarily a decrease in precision since there is a small probability for a few strong echoes per record. These have a strong weight in the least-squares adjustment which might compensate the effect of the random modulation. Gracheva et al. (1978) have shown that turbulence theory in the weak regime predicts a log-normal probability density function (PDF) for intensity fluctuations. According to Strohbehn (1978), in the strong regime the PDF becomes rather exponential. Such a PDF is thus likely in aerial, and even more in spatial, configurations. However, a statistical analysis for this phenomenon would be useful for optimizing instrumental parameters, such as beam divergence, pulse repetition frequency, and aerial survey duration (or number of satellite passes). Note that for the specific experiment considered below, speckle fluctuations were predominant owing to the use of a ground plate for achieving the laser beam divergence (Bock et al. 1997). Such intensity statistics is also of exponential PDF (Goodman 1975).

3.2 Laser transmitter

Wavefront distortions in laser beams have been well known to the SLR community (Degnan 1985). Historically, they were among the most limiting instrumental error source since biases up to a few nanoseconds were observed in various Q-switched lasers. These biases are approximately proportional to the pulse duration of the laser. Hence, mode-locked lasers are generally preferred since they provide pulse durations as short as 20 ps. We performed our own investigation of this phenomenon in different lasers too. For instance, we reported biases of 2 ns (30 cm), at half intensity, for a 5-ns Q-switched, unstable cavity, Nd:YAG laser and 50-ps (7.5 mm) for a 100-ps mode-locked laser (Bock et al. 1995). These biases had a systematic behavior in the short term, typically a few minutes, after which the spatial distribution changed significantly. They exhibited a nearly quadratic profile as a function of the transverse coordinate in the beam. Though it would be tempting to account for these systematic errors in the forward model, it is likely that the adjustment of related parameters would not be efficient. Instead, we propose to compensate for these effects (at least partly) through the adjustment of an offset in the vehicle trajectory. In Sect 5.4 it will be shown that trajectory offsets produce cumulative errors resulting in a catenary-curve-like distortion in CCR coordinates. In fact, laser biases produce similar cumulative errors peaking at the center of the network. This thus leaves the possibility to compensate simultaneously for both error sources by adjusting vehicle trajectory offsets. Hence, the 7.5-mm biases reported for our 100-ps laser might not be critical. This assumption will actually be confirmed from the experimental results presented later.

3.3 Receiver electronics

With our system a high link budget is required in order to provide a sufficient SNR for the data processing to be efficient. Contrary to most laser ranging systems (e.g., Bar-David 1969), with our system the fundamental temporal uncertainty owing to photon statistics limitation is negligible (echoes contain at least 10^4 photons). Consequently, instrumental error sources are predominant, namely in the receiver electronics.

3.3.1 System biases. Biases in the detection stage which exhibit a dependence on signal strength will be referred to as system biases. Such biases stem from nonlinearity in the detection stage electronics which produce distortions in pulse waveforms and hence time-of-arrival delays. They arise in the photodiode and amplifier, and become significant only for strong signal. As the signal magnitude fluctuates, biases and standard deviations in range measurements increase. An experimental characterization of our detection stage revealed that this effect was predominant in the amplifier, where it exhibited a quasi-linear relationship with a slope of 0.5 m/V. It is thus likely to produce decimeter ranging errors. When individual range measurements are corrected for this effect, the observed scatter is actually limited by the effect of electrical noise. Relative ranges exhibit then a nearly Gaussian distribution (Bock 1996).

3.3.2 Electrical noise and signal sampling. Additive electrical noise has contributions from photodiode, amplifier, and oscilloscope. However, with the current instrument, the latter two are predominant (Bock et al. 1997). Signal aliasing, owing to sampling in the oscilloscope, has a contribution that can be included as an additive error. The effect of both error sources on ranging performance has been assessed theoretically, assuming additive electrical noise is of Gaussian PDF

while signal sampling is of uniform PDF. The following expression has been found for the single-shot standard deviation, with a cross-correlation time-of-arrival estimator (Bock et al. 1997),

$$\sigma_\rho^2 \approx \left(\frac{K}{\mathrm{SNR}}\right)^2 + \sigma_a^2 \qquad (1)$$

where SNR $= a/\sigma_n$ is the signal-to-noise ratio, σ_n^2 the noise variance, a the magnitude of the measured pulse, K a waveform-dependent parameter and σ_a^2 the signal aliasing variance. With the aforementioned system, SNR ~ 100, $K = 0.3$ m, and $\sigma_a = 3$ mm, hence $\sigma_\rho = 4.2$ mm. A major interest of Eq. (1) is that the single- shot accuracy of each PR measurement can be predicted, assuming K and σ_n^2 have been calibrated previously.

Additionally, signal quantification, associated to signal sampling, also produces waveform distortions. For the case of a signal which magnitude matches the oscilloscope caliber (typically at the half range), this effect is negligible. Signal sampling also produces an uncertainty in each and every sample epoch, which is related to the clock stability. For our system it is at the picosecond level, and is thus negligible.

Two instrumental parameters are thus critical for maintaining a high ranging accuracy: SNR and K. They depend predominantly on the performance of the detection stage. For instance, to the first order, K is a function of the rise time of the measured pulses. Hence, the instrument can be optimized on the basis of a minimization of σ_ρ.

3.4 Budget of ranging accuracy

3.4.1 Theoretical assessment. Table 1 summarizes the effect of the described error sources, classified as random, systematic, and outliers. With the current system and signal processing, the budget of random errors in PR measurements is of 4.3 mm (single-shot), assuming an SNR of 100. Random errors are the less restrictive since the ranging uncertainty is reduced as $N_{\mathrm{Meas/CCR}}^{-1/2}$. The precision of estimates in CCR coordinates also follows this dependence when $N_{\mathrm{Meas/LS}}$ is large enough. On the other hand, systematic errors do not vanish as N_{Meas} is increased. They can either be reduced instrumentally (laser pulse duration), corrected numerically (a priori correction of receiver biases and mean PD) or compensated in the adjustment (laser biases). Additionally, outliers must be detected and rejected with the help of a proper signal processing strategy (Sect. 2.3.3).

Note that the effect of laser biases on actual measurements is difficult to predict, since it is a function of position in the beam pattern. The value of 7.5 mm reported in Table 1 is characteristic for a stationary beam pattern, whereas in experimental configurations the beam sweeps across the CCR network and is modulated by scintillation and/or speckle. Hence, it is likely that laser biases contribute partly to the random scatter, leaving a smaller systematic error component.

3.4.2 Experimental assessment. Up to now, three terrestrial experiments have been conducted which were characterized by different path lengths (100 m, 500 m, and 1 km), sources of beam divergence (ground glass plate and diverging lens, i.e., producing speckle effects or not), and turbulence regimes (winter and summer, i.e., weak or strong regimes). Since in these experiments paths were almost horizontal, only an approximate PD correction was applied, which assumed homogeneous index of refraction. Neglecting the differences in height between CCRs might contribute submillimeter errors in position estimates. Cross-correlation and least-squares deconvolution were used identically as time-of-arrival estimators.

Figure 4 compares observed with predicted single-shot accuracies in relative range versus SNR. The former is the RMS fluctuation in differential PR estimates, while the latter is computed from amplitude estimates with Eq. (1). One can see that both estimates for ranging accuracy agree fairly well. This reflects that instrumental

Table 1. Summary of error sources in estimates of PR

Error sources	type	scale	conditioning parameters
1. Atmosphere			
atmospheric delay correction	systematic	<1 mm, for 1 °C deviation	micro-meterological effects
pathlength fluctuations	random	<1 mm, for $C_n^2 = 10^{-14}$ m$^{-2/3}$	turbulence parameter, C_n^2
scintillation	random	shot-to-shot SNR fluctuations	C_n^2 and SNR
2. Laser transmitter			
wavefront distortion	systematic and random	<7.5mm at FWHM, for 100-ps pulse	Transverse mode build-up (see text)
3. Receiver			
Biases in the amplifier	systematic	negligible, after numerical correction	signal strength
electronic noise	random	~3 mm, for SNR = 100	K, SNR
signal aliasing	random	<3 mm, for a 1-ns sampling period	sampling period, receiver rise time
4. Wide-angle ranging			
pulse-shape overlap	outlier	negligible with signal deconvolution estimator and proper data sorting	receiver impulse response and rise time

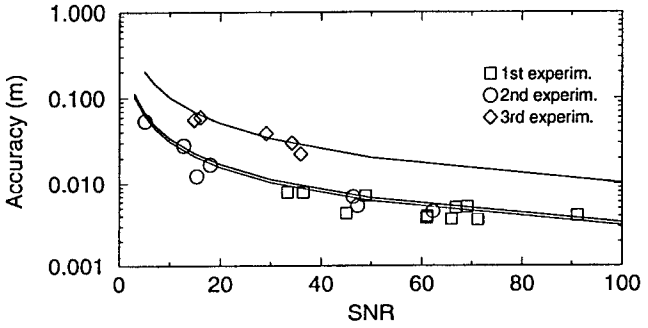

Fig. 4. Comparison between measured and predicted single-shot precision in relative ranges, versus SNR, for three ground-based experiments

biases (mostly from the amplifier) are properly corrected and that outliers are effectively rejected. For the case of experiments #2 and #3, the laser beam was smoothly swept about its normal direction in order to acquire data from an extended part of the CCR network. As a consequence, the observed scatter in relative ranges should include a contribution of laser biases. However, since observed and predicted accuracies show good agreement, it seems this contribution is small. Instead, measurements performed in stationary case (experiment #1) revealed small bias fluctuations of about ±3 mm in the long term (Bock et al. 1997). For the campaign analyzed in Sect. 6, it will be shown, however, that the effect of laser biases can be neglected, owing to the compensation by vehicle offsets.

Therefore, it will be assumed in the following that relative ranging errors are essentially random with a zero-mean Gaussian PDF. Only small biases are expected, owing to PD in aircraft measurements and residual laser biases.

4 Mathematical formulation of multilateration

4.1 Introduction

A method for dealing with general inverse problems has been proposed by Tarantola (1987), who stated that a rigorous manner for describing information is to use probability densities. The PDF for a posteriori information, i.e., the solution for the inverse problem, is given by the product of PDFs for a priori information, observational information, and physical model. Instead of the a posteriori PDF, the maximum likelihood (maximum of a posteriori PDF) is usually retained as the solution for the inverse problem. For the special case when all three sources of information are of zero-mean, Gaussian PDF, the a posteriori PDF is also Gaussian and is completely described by mean and covariance. Maximum and mean are then equal to the classical least-squares solution. However, it should be emphasized that the least-squares estimator is optimal only if all PDFs are Gaussian; in particular observations should be free of outliers. Moreover, in the case when PDFs are not of zero-mean, the solution might be strongly biased.

For this reason, all sources for systematic errors must be taken into account: PROs (Sect. 2.3), biases in PR measurements (Sect. 3) and systematic errors in a priori vehicle trajectory (see the following). Those errors are either adjusted, through proper parameterization, or compensated.

4.2 Forward model

Formally, the multilateration problem can be described by the following unknowns: locations of CCRs, U_i, locations of the vehicle, $\mathbf{V}_j$, and PROs, b_j, where $i = 1, \ldots, N_{\mathrm{CCR}}$ and $j = 1, \ldots, N_{\mathrm{LS}}$. Let $\mathbf{p}$ denote the vector parameter to be adjusted. The observation equation relates $\mathbf{p}$ to the PR observable, ρ_{ij}, between CCR #i and LS #j, according to

$$\rho_{ij} = \mathrm{PR}_{ij}(\mathbf{p}) + e_{ij} \tag{2}$$

where $\mathrm{PR}_{ij}(\mathbf{p}) = d_{ij}(\mathbf{p}) + b_j$ is the forward model for PRs and e_{ij} the combination of measurement and model errors. The straight-line distance between $\mathbf{U}_i$ and $\mathbf{V}_j$ is $d_{ij}(\mathbf{p}) = [(U_{xi} - V_{xj})^2 + (U_{yi} - V_{yi})^2 + (U_{zi} - V_{zj})^2]^{1/2}$ where coordinates are expressed in a common reference frame. As stated in the previous section, as long as system biases are properly corrected and outliers detected, measurement errors can reasonably be described by a random variable of zero-mean Gaussian PDF. The standard deviation for e_{ij} can be predicted according to the budget for error sources [see Table 1 and Eq. (1)]. It will also be assumed that the e_{ij} are uncorrelated.

For long ranges (typically above a few hundreds of meters), $\mathrm{PR}_{ij}(\mathbf{p})$ can be linearized around an a priori solution, $\mathbf{p}_0$. Equation (2) can thus be reduced to the following vector form

$$\mathbf{r} = \mathbf{A}\Delta\mathbf{p} + \mathbf{e} \tag{3}$$

where $\mathbf{r}$ is composed of a priori range residuals, $r_{ij} = \rho_{ij} - \mathrm{PR}_{ij}(\mathbf{p}_0)$, $\mathbf{A}$ is the partial derivative matrix calculated for $\mathbf{p}_0$, $\Delta\mathbf{p} = \mathbf{p} - \mathbf{p}_0$ is the solved parameter difference, and $\mathbf{e}$, again, is the combination of measurement and model errors. Hence, for the case when the linearization becomes inadequate, the actual PDF for e_{ij} may deviate from a zero-mean Gaussian model. Nevertheless, an iterative method may then be applied for solving the nonlinear inverse problem, starting with $\mathbf{p}_0$.

4.3 A priori information

In fact the prior solution, $\mathbf{p}_0$, represents an additional source of information which might be used for estimating $\mathbf{p}$, though of much lower weight than observables. A model for the PDF in $\mathbf{p}_0$, especially for vehicle trajectory, is therefore required. The uncertainty in relative vehicle coordinates is usually considered to be of ~50 cm with single-frequency GPS receivers using both PR and phase measurements (e.g., Sercel). However, an assessment of accuracy in relative coordinates computed

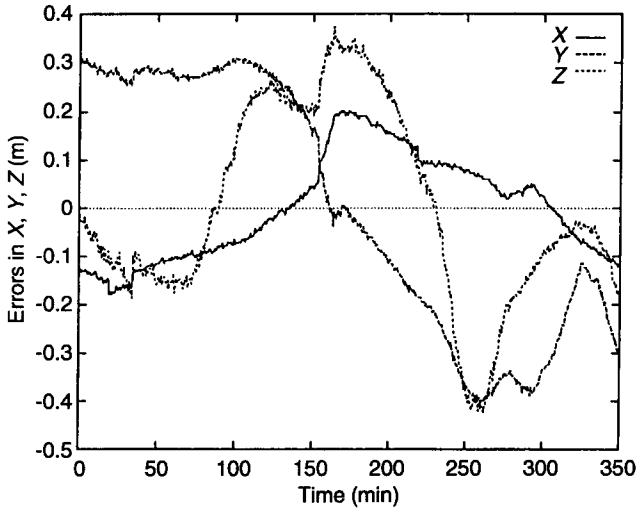

Fig. 5. Errors in estimates of relative coordinates from DGPS measurements computed with trajectography software. Baseline of the two (fixed) ground-based stations is of 500 m

from two ground-based fixed points showed that there is typically a strong low-frequency component on which is superimposed a weaker high-frequency component (see Fig. 5). While the former actually produces errors up to 50 cm (peak-to-peak), the latter is only of ~5 cm RMS. Obviously, a zero-mean Gaussian random process is not adequate for modeling such a non-stationary signal. However, on time-scales of order 10–15 min, such as for the ground-based experiment to be analyzed later, a linearly time-dependent model would account properly for the low-frequency component. This deterministic model can be included in the vector parameter $\mathbf{p}$ as a global offset, $\overline{\mathbf{V}}$, and a global drift, $\dot{\overline{\mathbf{V}}}$. Hence, the model for instantaneous vehicle locations, $\mathbf{V}_j$, becomes $\mathbf{V}_j + \overline{\mathbf{V}} + \dot{\overline{\mathbf{V}}}(t_j - t_0)$, where $(t_j - t_0)$ is the time since the beginning of the experiment. An additive white noise of Gaussian PDF would be reasonable for modeling the high-frequency component, with an a priori uncertainty of $\sigma_v = 5$ cm. On time-scales of the order of hours, such as for an aircraft experiment, a single set of linear-model parameters would not be accurate enough. There, each flight-path leg over the network should have independent linear-model parameters.

4.4 Inverse problem solution

Since both errors in range measurements and a priori information are described by zero-mean Gaussian PDFs, the weighted least-squares estimator is optimal for the maximum likelihood criterion, i.e.

$$\min_{\mathbf{p}} \left[S(\mathbf{p}) = (\mathbf{e}^{\mathrm{T}} C_{ee}^{-1} \mathbf{e} + \Delta\mathbf{p}^{\mathrm{T}} C_{pp}^{-1} \Delta\mathbf{p}) \right]$$

where C_{ee} and C_{pp} are the prior covariance matrixes for $\mathbf{e}$ and $\mathbf{p}_0$, respectively. The analytical solution, $\hat{\mathbf{p}}$, for this problem is given by the following expression (e.g., Tarantola 1987)

$$\hat{\mathbf{p}} = \mathbf{p}_0 + (\mathbf{A}^{\mathrm{T}} C_{ee}^{-1} \mathbf{A} + C_{pp}^{-1})^{-1} \mathbf{A}^{\mathrm{T}} C_{ee}^{-1} \mathbf{r} \qquad (4)$$

The posterior covariance, $C_{\hat{p}\hat{p}} = (\mathbf{A}^{\mathrm{T}} C_{ee}^{-1} \mathbf{A} + C_{pp}^{-1})^{-1}$, gives an insight to the theoretical accuracy of the estimated parameters. However, it measures the actual accuracy only if there are neither outliers nor systematic errors in the data. Therefore, we have put much effort in the parameterization of the problem and in the validation of our algorithm especially for outlier detection.

4.5 Adjustment procedure

Though the posterior covariance appears explicitly in the analytical solution of Eq. (4), it is not necessarily required for computing $\hat{\mathbf{p}}$. Instead, a Cholesky decomposition is used, since the square matrix to be inverted is both symmetric and positive definite. Owing to the size of the linear problem to be solved (of order $4 \times N_{\mathrm{LS}}$), a least-squares algorithm has been implemented that eliminates unknowns related only to LSs, i.e., $\mathbf{V}_j$ and b_j, when the related observations are added to the normal matrix, $\mathbf{B} = \mathbf{A}^{\mathrm{T}} C_{ee}^{-1} \mathbf{A}$. This is possible since every element of $\mathbf{B}$ is obtained by a summation over the number of observations. Hence, the final normal matrix is only composed of $\mathbf{U}_i, i = 1, \ldots, N_{CCR}$, and trajectory error model parameters, i.e., $\overline{\mathbf{V}}$ and $\dot{\overline{\mathbf{V}}}$ for the linear case. The Cholesky decomposition of the final normal matrix is consequently faster. However, LS-related unknowns are only estimated from a priori CCR coordinates and then eliminated. Hence, the estimates of vehicle coordinates are not known a posteriori. Additionally, a few iterations might be necessary in order to yield estimates of CCR coordinates which are independent of a priori vehicle trajectory.

5 Analysis of a ground-based experiment by numerical simulations

5.1 Outline

A ground based experiment has been conducted at Combs-la-Ville, near Paris, during December 1995. This experiment was implemented as a two-dimensional terrestrial configuration (see Fig. 6). A quasi-linear network, composed of 23 CCRs, was spread over a 725-m-long and 20-m-high hillock. The ranging system was operated onboard a small van from a nearly parallel road located 435 m away. This experiment simulated approximately an aircraft experiment. However, it was specific according to the following remarks:

1. Vertical coordinates of both CCRs and vehicle trajectory were strongly unresolved. This results from the fact that almost all CCRs were at the same height, on nearly a straight line. The vehicle trajectory consisted in a single linear eastward pass ($x > p$). All the measurements were thus performed in a nearly horizontal plane.
2. Errors in X- and Y-coordinates are strongly correlated owing to an eastward tilt of the laser beam which is required in order to get data from the beginning of the vehicle trajectory. It is thus necessary to distin-

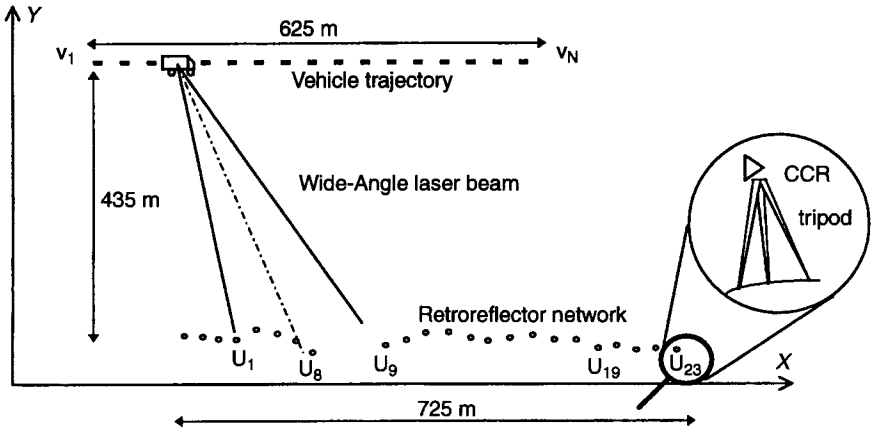

Fig. 6. Configuration for the ground-based experiment at Combs-la-Ville, France, 1995

guish between radial and transverse coordinates rather than X and Y.

3. The uncertainty in transverse coordinates of CCRs and vehicle trajectory are much higher than in radial coordinates, as a consequence of the low beam divergence. For instance, a 10° beam divergence (at $1/e^2$ intensity), yields $N_{\text{Meas/LS}} \sim 5$.

From these considerations, it appears pertinent to study the effects on the accuracy in radial and transverse CCR coordinates of the following error sources and experiment configurations:

1. Unresolved parameters: vertical coordinates and reference CCR locations.
2. Experiment configuration: tilt and divergence of the laser beam.
3. Systematic errors in vehicle trajectory: offsets and drifts.
4. Pseudo-range offsets varying from shot to shot.

These effects are considered in Sects. 5.2–5.5. The posterior covariance matrix is intensively used for analyzing correlation coefficients and standard deviations of the adjusted parameters. A methodology for the data processing in the ground-based experiment is derived and the extension to aerial configurations, when the radial coordinate is the vertical, is discussed in Sect. 6.

The data generated for the analysis have the following common characteristics: $N_{\text{CCR}} = 23$ and $N_{\text{LS}} = 10^3$. Measurement noise and uncertainties in a priori locations are simulated by an additive quasi-random signal of Gaussian PDF. As will be shown in Sect.5.3, with a 10° beam divergence the constraints relating the two segments composed of CCRs #1 to 8 and #9 to 23 are very weak. Hence, the CCRs at the extremities of those are fixed with a priori uncertainties of 10^{-4} m. Moreover, for the second segment CCR #18 has been fixed because too few measurements are achieved for CCRs #18 to 23 with a constant tilt angle of 15°. Note that the effect of PRO adjustment is not considered in Sects. 5.2–5.4 but is studied separately in Sect. 5.5.

5.2 Effects of unresolved parameters

The main unresolved parameters are all vertical coordinates and fixed (reference) CCR coordinates. In this subsection it is shown that their effect on estimates of CCR coordinates is strongly repetitive which is thus overcome by considering between-epoch coordinate differences.

Here, PR data are simulated for the case of an unlimited beam divergence, from which it follows that $N_{\text{Meas/LS}} = N_{\text{CCR}}$ and $N_{\text{Meas/CCR}} = N_{\text{LS}}$. A priori uncertainties in vehicle and CCR coordinates are of 10 cm, independently of the measurement geometry. PROs are fixed by setting a small a priori uncertainty of $\sigma_b^{(\text{prior})} = 10^{-5}$ m.

5.2.1 Unresolved vertical coordinates. Since vertical coordinates are unresolved, prior and posterior precision in Z are almost equal. Let $\rho_{YZ} = \frac{c_{YZ}}{\sigma_Y \sigma_Z}$ denote the correlation between the Y-and Z-coordinates of a particular CCR, where c_{YZ} is the posterior covariance, and σ_Y and σ_Z are posterior standard deviations referred to as the (theoretical) precision in Y and Z. For instance, the approximate relationship between posterior errors in δY and δZ is

$$\delta_Y \approx \rho_{YZ} \frac{\delta_Z}{\sigma_Z} \sigma_Y = \frac{c_{YZ}}{\sigma_Z^2} \delta Z \tag{5}$$

From simple geometrical considerations (see Fig. 6) it can be predicted that ρ_{XZ} is much lower than ρ_{YZ}, except for fixed CCRs. This is confirmed in Fig. 7, where ρ_{XZ} and ρ_{YZ} are compared for two different values of $\sigma_Z^{(\text{prior})}$, the prior uncertainty in Z.

For the case when $\sigma_Z^{(\text{prior})} = 0.1$ m, $\rho_{YZ} \approx 1$, i.e., δY and δZ are likely to be linearly dependent. The high correlation between these parameters indicates that most of the scatter in Y stems from posterior errors in Z. Errors in Y are actually predictable to a good accuracy with the help of Eq. (5), as is shown in Fig. 8. Hence, the ultimate precision in Y is given by the RMS difference between Y and δY, denoted by $\hat{\sigma}_{Y-\delta Y}$. Table 2 shows that the ultimate precision in Y is of 0.5 mm, whereas the effect of Z reduces this accuracy to about 3 mm, as predicted by σ_Y or $\hat{\sigma}_Y$. Figure 8 shows that errors in Y

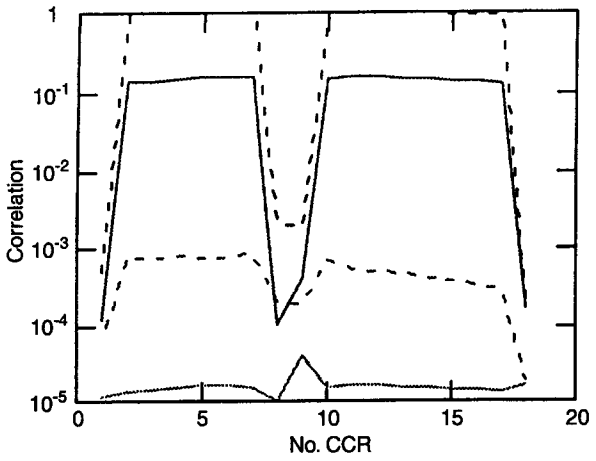

Fig. 7. Posterior correlation between X and Z (solid lines), and Y and Z (dashed lines), owing to errors in Z. Upper curves are for $\sigma_z^{(prior)} = 10^{-1}$m and lower curves for 10^{-5}m

are mostly repetitive. Most of the contribution of Z on Y can then be removed when differential coordinates are considered. Those are quantified in Table 2 by $\hat{\sigma}_{\Delta Y}$, the RMS difference between two experiments. Note that since ρ_{XZ} is relatively small, the contribution of errors in Z on X is negligible, which is illustrated in Fig. 8 and Table 2.

The case when $\sigma_Z^{(\text{prior})} = 10^{-5}$ m provides another way for estimating the ultimate precision. There, the theoretical precision , σ_Y, assumes that vertical coordinates are perfectly known . Hence, the value predicted for σ_Y does not include the contribution of actual errors in Z. Table 2 shows that $\sigma_Y = 0.6$ mm is predicted, which is compatible with the previous estimate for the ultimate precision in Y. Identically, the correlation ρ_{YZ} also assumes errors in Z are negligible, from which a value of 10^{-3} is predicted. This value is evidently much smaller than that of the previous case. However, RMS values computed from observed errors are roughly independent of $\sigma_Z^{(\text{prior})}$. Though the actual prior uncertainty in Z is of order 10 cm, vertical coordinates will be fixed for the simulations presented in the following, in order that σ_Y predicts properly the ultimate precision in Y. Identically, when $\hat{\sigma}_{\Delta Y} \sim \sqrt{2} \times \sigma_Y$ is observed from experimental data it can be stated that systematic biases are properly eliminated. The ultimate precision is thus achieved in differential coordinates.

Note that here only the case of unlimited beam divergence has been considered. When the beam divergence is decreased, theoretical precision and correlation also decrease. For instance, a 10° beam divergence provides a correlation between 0.6 and 0.8. Nevertheless, the present conclusions about the effects of unresolved Z on precision remain unchanged.

5.2.2 Unresolved reference CCRs. In these simulations, vertical coordinates of both CCRs and vehicle trajectory are noise-free, while all CCR coordinates are noised, especially fixed CCRs. The results basically lead to the same conclusions as for unresolved Z. A strong correlation appears between the coordinates of fixed CCRs and other CCRs of the same segment. Errors predicted in X and Y are quite strong, whereas they are negligible in Z (whether these latter coordinates were fixed or not). The errors act as a coherent spatial distortion of the solution for X- and Y-coordinates. Fortunately, a high

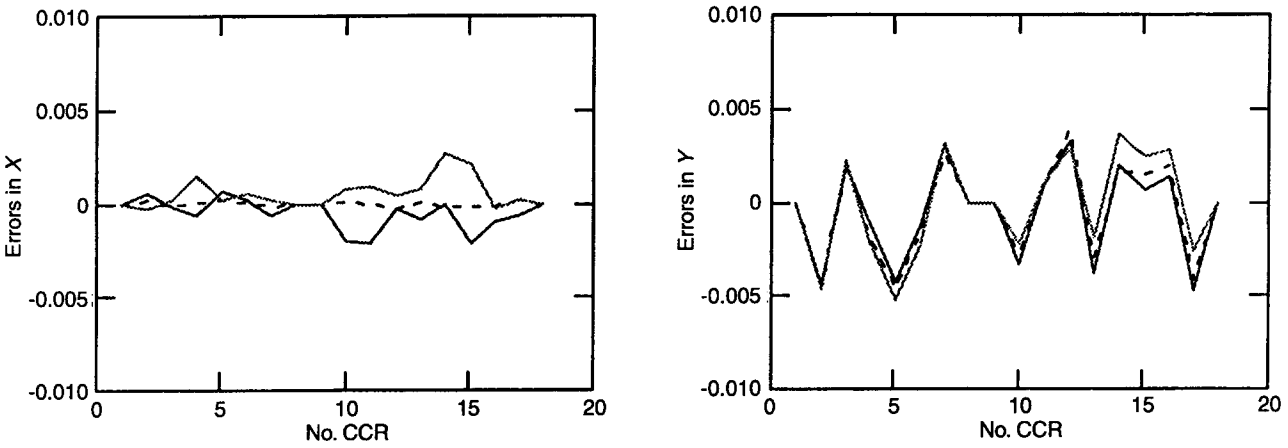

Fig. 8. Comparison between observed (solid lines) and predicted (dashed lines) errors in X (left) and Y (right) owing to errors in Z. Observed errors for two different experiments are compared (light and dark solid lines)

Table 2. Theoretical precision (σ_X, σ_Y) and observed uncertainty for a single solution ($\hat{\sigma}_X, \hat{\sigma}_Y$), a single solution corrected for Z-correlated errors ($\hat{\sigma}_{X-\delta X}, \hat{\sigma}_{Y-\delta Y}$), and the difference between two solutions ($\hat{\sigma}_{\Delta X}, \hat{\sigma}_{\Delta Y}$). Data simulated for unlimited beam divergence. Values computed over CCR #1 to #18

$\sigma_Z^{(\text{prior})}$	σ_X	σ_Y	$\hat{\sigma}_X$	$\hat{\sigma}_Y$	$\hat{\sigma}_{X-\delta X}$	$\hat{\sigma}_{Y-\delta Y}$	$\hat{\sigma}_{\Delta X}$	$\hat{\sigma}_{\Delta Y}$
10 cm	1.1 mm	3.2 mm	1.1 mm	2.8 mm	1.1 mm	0.5 mm	2 mm	1.2 mm
0.01 mm	1.1 mm	0.6 mm	1.1 mm	2.9 mm	1.1 mm	0.5 mm	2 mm	1.1 mm

repeatability is achieved, provided fixed points are actually steady. Again, by differentiating two solutions, systematic errors in reference CCR locations vanish and the observed accuracy becomes compatible with the theoretical precision. For instance, a precision of $\sigma_X = 1.1\,\text{mm}$ and $\sigma_Y = 0.6\,\text{mm}$ is still predicted and $\hat{\sigma}_{\Delta X} = 1.9\,\text{mm}$ and $\hat{\sigma}_{\Delta Y} = 1.1\,\text{mm}$ is observed. These values are consistent with the results reported in Table 2. When the beam divergence is reduced, theoretical precision and observed accuracy remain again compatible.

5.3 *Effects of experiment configuration*

The effects of two important characteristics of the ground-based experiment on positioning precision are analyzed here: first the influence of a global tilt in the laser beam direction and, second, the influence of the laser beam divergence. Three different values for the beam divergence, α, are considered: unlimited, 20°, and 10°. (Note that the latter two also include a 15° eastward tilt.) In order to get rid of the effect of the unresolved parameters analyzed above, here fixed CCRs and vertical coordinates of CCRs are not noised; and instead are fixed by means of 10^{-5}-m prior uncertainties. Observed errors depend thus only on instrument and experiment characteristics. The vehicle coordinates (X, Y, and Z) are noised with a zero-mean Gaussian noise of 50-cm standard deviation. Offset and drift parameters, $\bar{\mathbf{V}}$ and $\dot{\bar{\mathbf{V}}}$, are fixed with priori uncertainties of 10^{-5} m and 10^{-5} m/LS, respectively. PROs are fixed by setting a small a priori uncertainty of $\sigma_b^{(\text{prior})} = 10^{-5}\,\text{m}$.

5.3.1 Laser beam tilt. Tilting the laser beam does not by itself produce errors in estimates of CCR coordinates. Instead, it introduces a strong correlation, ρ_{xy}, between errors in X and Y. Therefore it is more meaningful to analyze the results in radial and transverse coordinates. In geodetic data analysis, accuracy is usually represented by confidence ellipsoids whose flatness increases with

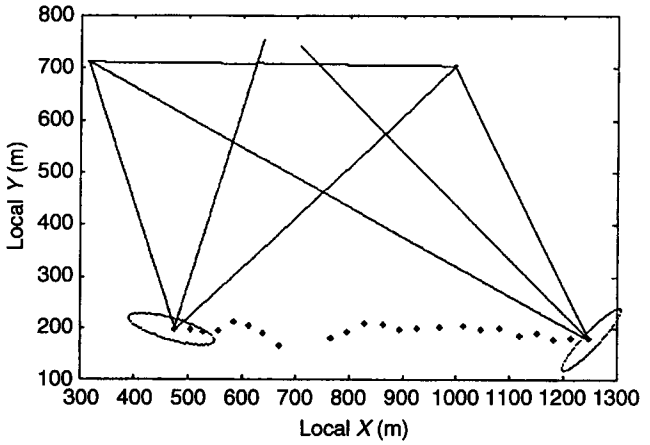

Fig. 9. Confidence ellipses for a simulation with unlimited divergence

correlation. Additionally, a large uncertainty in the transverse coordinates results from a small divergence. Figure 9 shows schematically confidence ellipses for the case of unlimited divergence. There, the orientation of the ellipses depends on the mean measurement angle which is different for all CCRs. However, when the divergence is strongly limited, all orientations tend toward the tilt angle of the laser beam (provided it is constant), and the results can be analyzed in a tilted reference frame which axes will be denoted by R and T, standing for radial and transverse (coordinates), respectively. In the actual experiment configuration, with $\alpha \sim 10°$ and a tilt of $\alpha \sim 20°$, the same strong correlation between errors in X and Y is expected for all CCRs.

5.3.2 Laser beam divergence. A reduction in α contributes to a decrease in precision for two reasons. First, a reduction of $N_{\text{Meas/LS}}$, and therefore $N_{\text{Meas/CCR}}$ and N_{Meas}, would lead to a reduction in precision following the $N_{\text{Meas/CCR}}^{-1/2}$ relationship. Second, a reduction in the field of view might lead to nearly critical configurations. Unfortunately, the experiment when $\alpha = 10°$ is nearly critical, according to $N_{\text{Meas/LS}} \sim 5$. As a result, the precision in T becomes much smaller than in R.

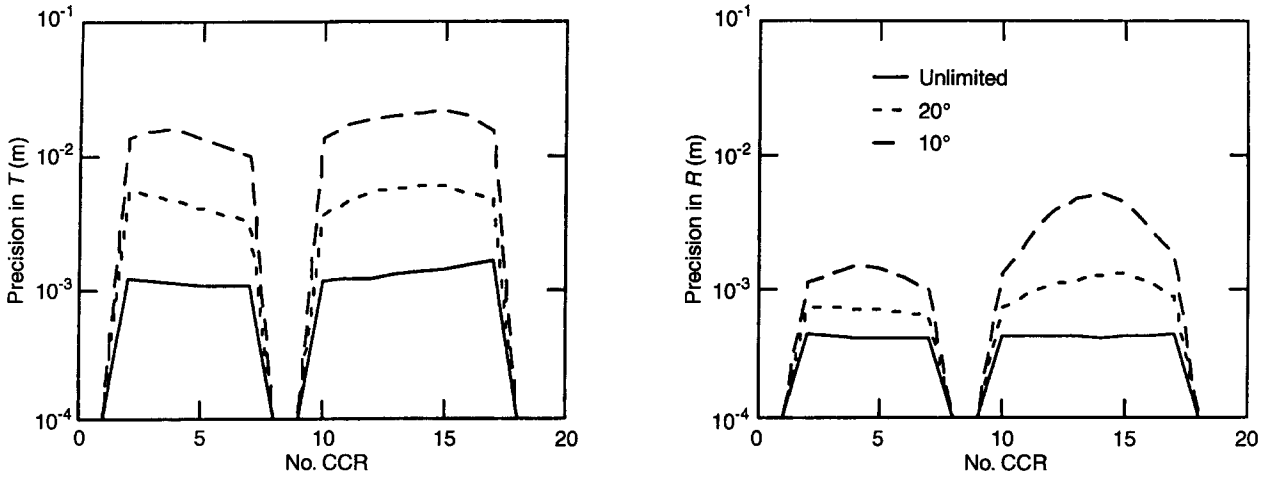

Fig. 10. Theoretical precision in radial and transverse coordinates of CCRs as a function of beam divergence

Table 3. Theoretical precision in radial and transverse coordinates (computed over CCR#1 to #18)

Beam divergence	N_{Meas}	σ_T	σ_R
unlimited	23 000	1.1 mm	0.6 mm
20°	10 134	3.8 mm	0.7 mm
10°	5164	16 mm	2.7 mm

Additionally, the reduction in precision is not properly predicted from $N_{\text{Meas/CCR}}$ alone, as is shown in Fig. 10 and reported in Table 3.

For the specific case when $\alpha = 10°$, $\sigma_p = 1$ cm and $N_{LS} = 10^3$, the precision in R is of 2.7 mm. Any additional information is thus welcomed for achieving a higher positioning precision. For instance, a reduction of the a priori uncertainty in vehicle locations has been considered. Estimating $\overline{\mathbf{V}}$ and $\dot{\mathbf{V}}$ is a possible way of reducing this a priori uncertainty to $\sigma_{\text{GPS}}^{(\text{prior})} \sim 5$ cm. This is considered in next subsection.

5.4 *Effects of systematic errors in vehicle trajectory*

The objective of adjusting a deterministic model for systematic errors in vehicle trajectory is motivated by two considerations. First, a higher positioning precision might be achieved for the case when $\alpha = 10°$. Second, since systematic errors in vehicle trajectory are actually suspected (see Fig. 5), the use of a least-squares adjustment method might lead to strong biases (see Sect. 4).

In this subsection, the pertinence of modeling offsets and drifts in vehicle trajectory is investigated. First, the a posteriori precision for these parameters is estimated. Then the effect of two different models on predicted and observed precision (in CCR coordinates) is analyzed. In the first model, referred to as model A, $\overline{\mathbf{V}}$ and $\dot{\mathbf{V}}$ are not included. However, $\sigma_{\text{GPS}}^{(\text{prior})}$ is assumed to be ~50 cm, which is compatible with actual peak-to-peak errors. In the second model, referred to as model B, $\overline{\mathbf{V}}$ and $\dot{\mathbf{V}}$ are actually modeled and adjusted, while $\sigma_{\text{GPS}}^{(\text{prior})} = 5$ cm.

The data are simulated according to the following specifications. Regarding PR data: $\sigma_\rho = 1$cm, $\alpha = 10°$ with a tilt of 15°. The vehicle trajectory includes either an offset or a drift along with a 5-cm random noise (in X, Y and Z). The trajectory offset is of 30 cm in X and −50 cm in Y, while the drift is of 0.5 mm/LS in X and −0.3 mm/LS in Y. The noise in CCR coordinates is of 10 cm (in X and Y). PROs are fixed by setting a small a priori uncertainty of $\sigma_b^{(\text{prior})} = 10^{-5}$m.

5.4.1 Precision in model parameters for trajectory biases. For the case of model B, the a posteriori precision for offsets and drifts can be estimated from the covariance matrix. For offsets, values of 9 and 4 mm in X and Y, respectively, are found. The precision for drifts is 0.02 and 0.008 mm/LS, respectively in X and Y. The higher precision in the Y component is due to the experiment configuration: with $\alpha = 10°$, the Y of the trajectory is relatively well constrained, while the X component is quite badly resolved. However, both components are considered to be sufficiently resolved for adjusting actual offsets and drifts with the aim of compensating biases in CCR coordinates at the 1-mm level.

Note also that the posterior correlation between either offsets or drifts and CCR coordinates is significant and reaches values up to 0.6. The pattern of the correlation follows roughly a catenary curve between fixed points. However, it is strongly fluctuating, depending mainly on a priori uncertainties of (random) trajectory errors and PROs.

5.4.2 Positioning precision with systematic errors in vehicle trajectory. The reduction of the a priori uncertainty in vehicle trajectory to $\sigma_{\text{GPS}}^{(\text{prior})} = 5$ cm yields a higher precision in radial and transverse estimates of CCR coordinates such as $\sigma_T = 9$ and $\sigma_R = 1.1$ mm (to be compared to those reported in Table 3 for $\alpha = 10°$). Some information is thus added from the a priori vehicle trajectory. In our case, the improvement in precision is additionally balanced because of the adjustment of offset and drift parameters (see Table 4). The a priori uncertainties for the latter have been fixed to $\sigma_{\text{offset}}^{(\text{prior})} = 1$m and $\sigma_{\text{drift}}^{(\text{prior})} = 0.5$ mm/LS. Ultimately, if the vehicle trajectory were perfectly known, the precision would be of $\sigma_T = 6$ mm and $\sigma_R = 0.7$ mm, which is only a moderate improvement with respect to the case when $\sigma_{\text{GPS}}^{(\text{prior})} = 5$ cm.

Results from different combinations of offsets and drifts in trajectory data and adjustment models are reported in Table 4. For the case of model A, the discrepancy between precision and RMS error is a measure of the strength of biases resulting from systematic errors in vehicle trajectory. Observed RMS errors are much higher than predicted from the covariance matrix which assumed zero-mean random errors. Note also the stronger effect of offsets or drifts in X on both σ_T and σ_R. For the case of model B, precision and RMS errors agree well. This confirms that offsets and drifts are ad-

Table 4. Theoretical precision and observed uncertainty in radial and transverse coordinates. Model A: $\sigma_{GPS}^{(\text{prior})} = 50$-cm random error; model B: $\sigma_{GPS}^{(\text{prior})} = 5$ cm + offset and drift. Errors: offset in $X = 30$ cm, in $Y = -50$ cm; drift in $X = 0.5$ mm/LS, in $Y = -0.3$ mm/LS

Systematic error in trajectory data	model for adjustment	σ_T	σ_R	$\hat{\sigma}_T$	$\hat{\sigma}_R$
offset in X	model A	16 mm	2.7 mm	66 mm	5.5 mm
offset in Y	model A	16 mm	2.7 mm	20 mm	1.9 mm
offset in X or Y	model B	11 mm	1.2 mm	8.6 mm	1.0 mm
drift in X	model A	16 mm	2.7 mm	47 mm	3.9 mm
drift in Y	model A	16 mm	2.7 mm	15 mm	1.5 mm
drift in X or Y	model B	11 mm	1.2 mm	8.3 mm	1.1 mm

justed with sufficient accuracy to remove the effects of trajectory biases.

From geometrical considerations, one can see that systematic errors in the X component of the vehicle trajectory produce cumulative errors in CCR coordinates, especially in Y. Owing to the fixed extremities, these errors tend to peak at the center of the network and are likely to exhibit approximately a catenary curve. The effect of systematic errors in the Y component of the vehicle trajectory is slightly different. There, the cumulative effect is smaller, but biases still appear in position estimates, however. This behavior is quantified in Table 4 and illustrated in Fig. 11 for the case when offsets in both X and Y are simulated and model A is used for the adjustment. (Note that with drifts one gets roughly the same results.) The errors follow roughly a catenary curve, except in the transverse coordinates of the second segment which exhibits a kind of higher-order mode. Errors of up to a few centimeters are observed in the radial coordinates of CCRs at the center of the segments. For the case of model B, the distribution of errors no longer exhibits a particular mode but is rather dependent on the particular realization of PR noise which is consistent with error-bars.

5.5 *Effects of PROs*

When PROs are adjusted, an information exchange arises between those parameters and trajectory coordinates, especially in the radial component for the case of a small beam divergence. This correlation depends strongly on the value for $\sigma_b^{(\text{prior})}$, and exhibits a minimum when $\sigma_b^{(\text{prior})} \sim \sigma_{\text{GPS}}^{(\text{prior})}$. Hence, in order to minimize this effect, a high a priori uncertainty in PROs such as $\sigma_b^{(\text{prior})} = 10$ m, is used, though the actual PROs are believed to be much smaller (see Sect. 2.3). The precision for offsets becomes then 3 and 8 cm, respectively, in X and Y while the precision for drifts becomes 0.05 and 0.15 mm/LS, respectively. The decrease in precision for these parameters is significant (compare to the values reported in the previous section). However, it is still sufficient for compensating the effect of actual biases in

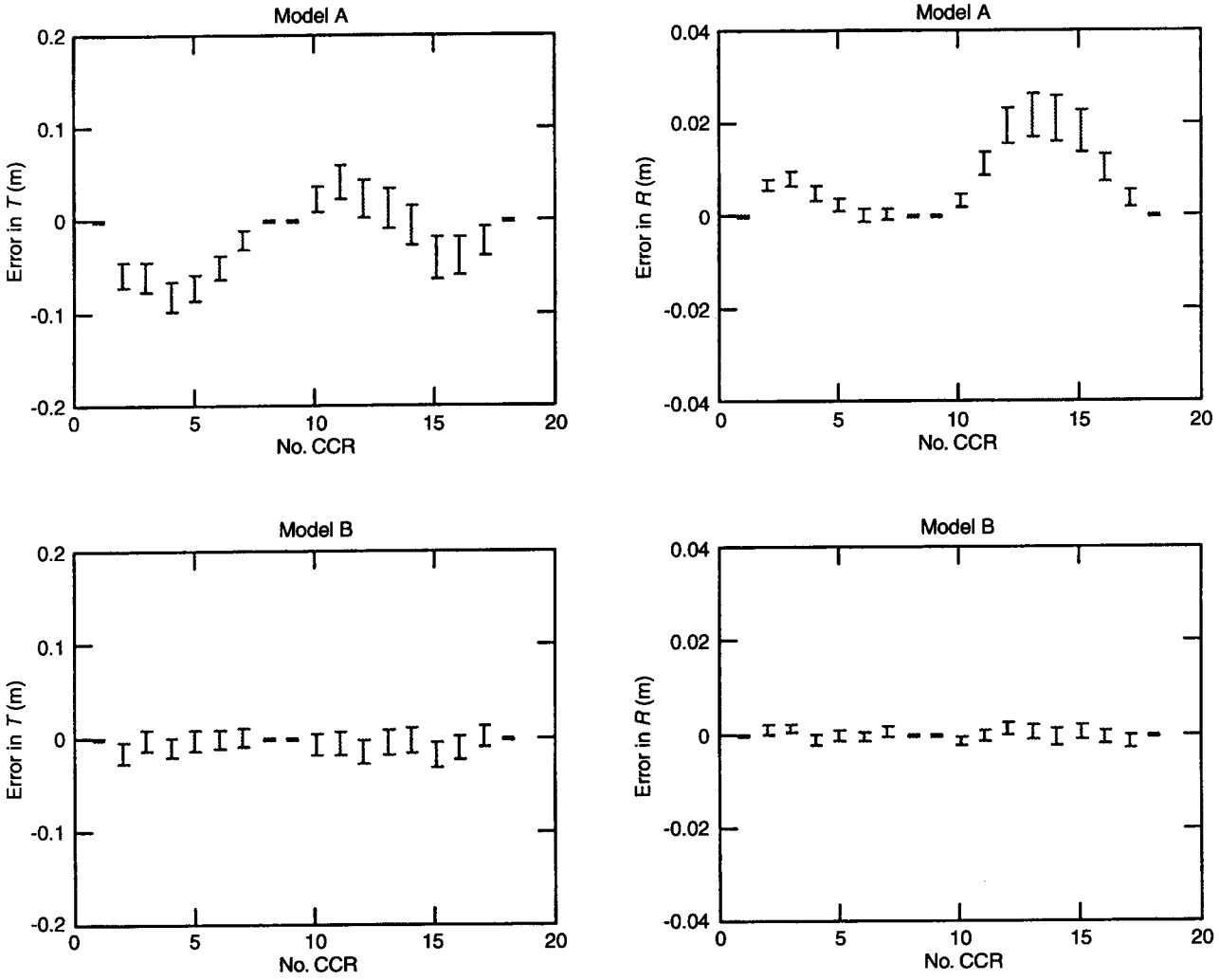

Fig. 11. A comparison between results (computed from a particular solution) for two models: A, a priori uncertainty in vehicle trajectory of 50 cm (random only); B, a priori uncertainty of 5 cm with offsets and drifts. Error bars at $\pm 1\sigma$, as predicted from the covariance matrix

the vehicle trajectory on CCR coordinates. This is partly due to the fact that, though the uncertainty in Y components is about three times that of the X components, the former has a smaller effect on CCR coordinates.

PROs contribute as one more unknown to be adjusted from PR measurements at each LS. The precision in coordinates of both vehicle and CCRs might thus be reduced when PROs are adjusted. However, with the specific experiment considered here, the decrease in precision remains small, though $\alpha = 10°$. Precision in estimates of CCR coordinates is of $\sigma_T = 12$ and $\sigma_R = 1.2$ mm (with model B and $\sigma_b^{(\text{prior})} = 10$ m). These values should be compared with those reported in Table 4, when $\sigma_b^{(\text{prior})} = 10^{-5}$ m. The smallness of the decrease in precision might be explained by the fact that the network is composed of two independent segments, of relatively small sizes, which requires that four CCRs be fixed. As a consequence, the vehicle trajectory is quite well determined and both PROs and vehicle coordinates are adjusted with a relatively good accuracy.

Note that here the model for PROs includes only a random component varying from shot to shot. A nonzero mean value in PROs would lead to systematic errors comparable to those produced by trajectory biases, when not modeled.

6 Ground-based experiment results

6.1 Measurements

The configuration of the experiment conducted at Combs-la-Ville, France, is shown in Fig. 6. The network was composed of $N_{\text{CCR}} = 23$ glass CCRs of 6 cm diameter, mounted on portable tripods. A beam divergence of $\alpha \sim 10°$ was achieved with a ground glass plate. The laser beam pattern produced an average number of echoes of 8, when the laser beam was slightly tilted. The tilt angle was $\sim 20°$ for the first segment and $\sim 30°$ for the second segment in order to acquire data from the whole network.

A priori locations of CCRs had been measured previously, by means of rapid-static DGPS, with single-frequency receivers (Sercel, NR-101). The vehicle trajectory was measured with the same receivers (0.6-s epoch interval). The single-shot ranging accuracy achieved during this experiment is between 3 mm and 10 cm (experiment #3 in Fig. 4). Atmospheric PD is only roughly corrected, by applying a constant scaling factor to the range measurements (cf. Sect. 3). However, a mean correction for instrumental biases is required since a mean PRO offset is not modeled.

During this campaign, CCRs and tripods had to be removed in the evening and installed again in the morning. Therefore, only data from the same day can be compared in order to estimate the positioning repeatability. Observed RMS errors are computed over the set of retroreflectors rather than over an ensemble of experiments. Note that for the case of actual geodetic surveys, concrete pillars would be used which would remain on the terrain as long as it has to be surveyed. Then, CCRs would be repositioned to less than 1 mm on the pillars before each survey.

6.2 Adjustment procedure

From the numerical simulation presented in the previous section, a methodology for data processing and interpretation has been defined for our specific ground-based experiment. Namely, the following a priori uncertainties for adjusted parameters have been retained: 1 m in vehicle trajectory offsets and 0.5 mm/LS for drifts; 10 cm in CCR coordinates; 5 cm in vehicle coordinates (random component); and 10 m in PROs. The uncertainty in PR measurements is predicted from Eq. (1). All vertical coordinates are fixed with an a priori uncertainty of 10^{-5} m. CCRs are fixed at the extremities of independent segments. Additionally, they are chosen in order to yield $N_{\text{Meas/CCR}} > 200$.

The two thresholds for outlier detection (see Sect. 2.3.3) are adjusted to the experimental data. A value of 4 m was effective for detecting pulse coincidences. Regarding CCR misidentification, the detection of threshold crossing in RMS a priori range residuals turned out to be quite effective. However, two iterations of the adjustment algorithm are operated. The first one is used to reject big outliers by means of a higher threshold, such as 10 cm, which is consistent with a relatively low false-alarm probability. A first estimate of mean parameters such as trajectory offsets and drifts results from this former adjustment. The second adjustment is performed with a lower threshold, such as 5 cm, from which accurate estimates of CCR coordinates are achieved. This simple outlier detection method might be further improved, however, by taking into account the time dependence of LSs. For example, a filtering method applied to the posterior residuals from the first iteration could be applied before performing the second adjustment.

6.3 Positioning precision

Results from two runs for each of two days of experimentation are reported in Table 5. In this experiment $N_{\text{Meas/Ls}} \sim 5$ owing to the combination of a small beam divergence, short range, and outlier detection. With such a small value for $N_{\text{Meas/LS}}$, information enhancement provided a small value for $\sigma_{\text{GPS}}^{(\text{prior})}$ is useful. The posterior precision in offsets is there of 5–10 cm, and ~ 0.05 mm/LS for drifts, from day I (see Table 5). During the second day of experimentation, geometrical configurations and system noise had changed significantly, which produced higher measurement and a priori uncertainties. For other experiments (not presented here), the conditions were even worse, and did not lead to stable solutions.

A first assessment of the repeatability is made from the two pairs of runs reported here. Table 6 shows the RMS differences between coordinates from two different runs. These agree well with (theoretical) precision pre-

Table 5. Results from the ground-based experiment: data volume and theoretical precision (radial and transverse CCR coordinates and vehicle offsets and drifts). Different days of experimentation are denoted by #I and #II while #1 and #2 denote runs performed during a given day

Run	N_{Meas}	$N_{Meas/CCR}$	$N_{Meas/LS}$	σ_T	σ_R	X-offset	Y-offset	X-drift	Y-drift
I-1	4 024	175	5	14 mm	1 mm	5.5 cm	6.4 cm	0.05 mm/LS	0.05mm/LS
I-2	8 579	373	4.8	13 mm	1 mm	9.7 cm	8.8 cm	0.04 mm/LS	0.05 mm/LS
II-1	7 262	315	5.1	20 mm	3.5 mm	13 cm	16 cm	0.06 mm/LS	0.09 mm/LS
II-2	5 827	253	5.2	26 mm	4 mm	17 cm	19 cm	0.14 mm/LS	0.12 mm/LS

Table 6. RMS differences in transverse and radial coordinates between runs

Solution difference	$\hat{\sigma}_{\Delta T}$	$\hat{\sigma}_{\Delta R}$
I-1–I-2	18 mm	1 mm
II-1–II-2	38 mm	2.3 mm

dictions from both the a posteriori covariance matrix (Table 5) and with the numerical simulations of the previous section (Table 3, for $\alpha = 10°$). Figure 12 shows differences in estimates of transverse and radial coordinates of CCRs, with error-bars at $\pm 1\,\sigma$ (where σ is the predicted standard deviation for each CCR). For both days the scatter is reasonably consistent with error-bars. This gives confidence to the instrumental solution proposed. Though 7.5-mm short-term biases are likely in the laser beam, they are not critical. It is believed that these biases are mostly compensated by the trajectory offset and that the residual errors both produce small biases, below 1 mm, and contribute to a small increase in scatter.

Note that only results for the second segment are represented. In fact the number of measurements for CCRs of the first segment was very small. The strong posterior uncertainty in these CCRs thus increased the

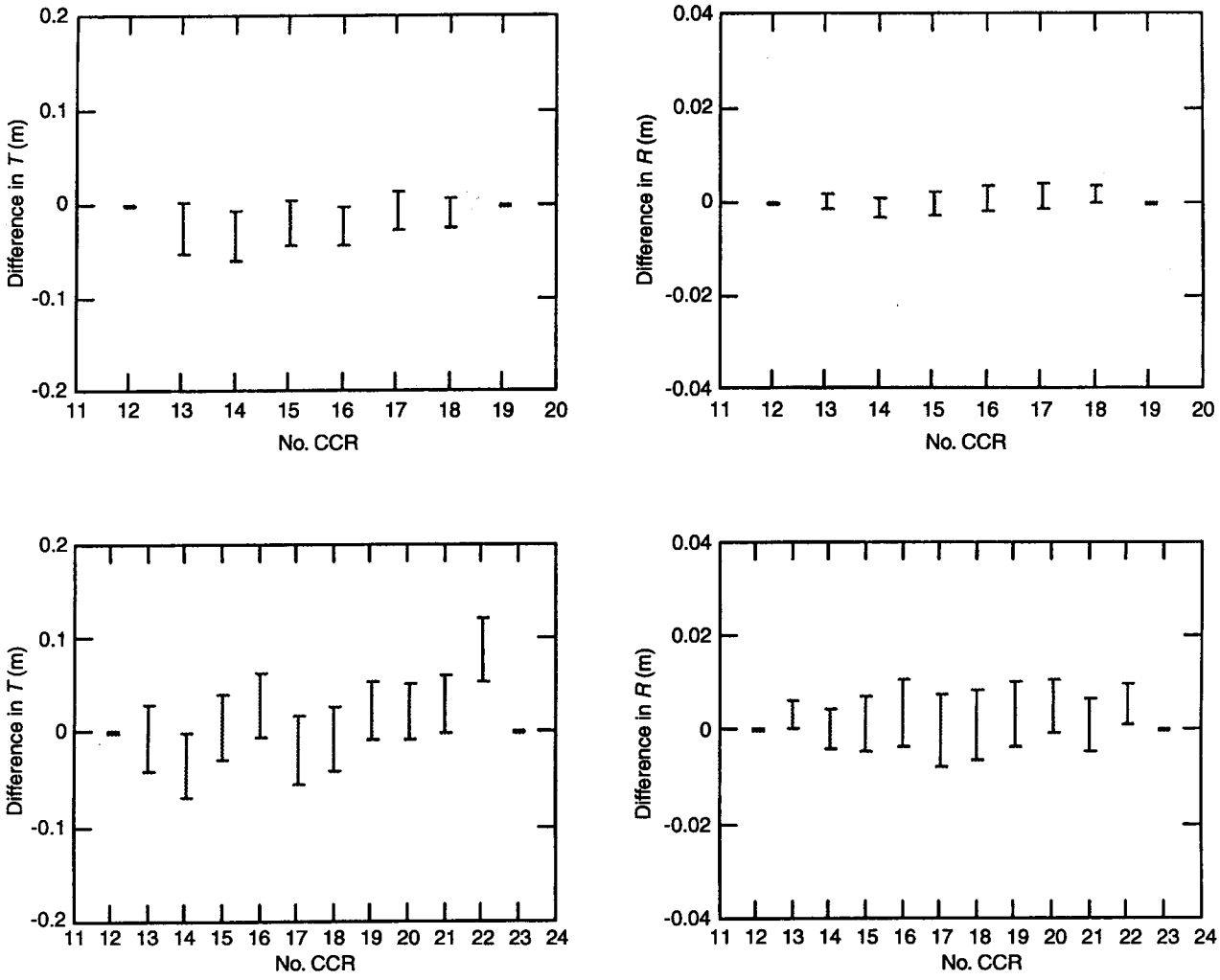

Fig. 12. Differential transverse and radial coordinateds of CCRs, between runs I-1 and I-2 (upper figures) and between runs II-1 and II-2 (lower figures). Error bars at $\pm 1\sigma$, as predicted from the covariance matrix

uncertainty in trajectory model parameters. Since these were common to both segments, strong biases remained in CCR coordinates. In order to make the solution stable, CCRs of the first segment were thus fixed.

7 Summary and discussion

A new geodesy technique, devoted to large (100 km^2) and dense (1 km^{-2}) networks of CCRs, has been described. It is based on the multialteration principle, in which simultaneous PR measurements are achieved with a divergent laser beam and a direct-detection system. Times of arrival, and therefore PRs, and amplitudes for echoes reflected for any transmitted laser pulse are estimated with a deconvolution method (least-squares adjustment). Single-shot ranging accuracies as low as 3 mm have been observed. It has been shown that system (electronic) noise is the predominant source of random errors in those estimates. Additionally, the effect of different systematic error sources has been assessed. It has been shown that system receiver biases and mean PD can be numerically corrected a priori (i.e., before resolution of the inverse problem). Outliers stemming from coincidence of echoes can be detected by a threshold crossing of the standard deviation in a priori range residuals.

A model for a priori knowledge has also been derived, especially for systematic errors in vehicle trajectory. Offsets of order 0.5 m with drifts of order 0.5 mm/LS have been reported from DGPS measurements. It is believed that efforts might be done in DGPS trajectography processing in order to reduce those biases. For instance, we recommend a more accurate correction for atmospheric refraction, e.g., including profiles or integrated content of water vapor. However, for data from current systems, a model composed of an offset and a drift would be valid for ~15 min. This is roughly the duration of either a flight-path leg in a typical aircraft experiment or a satellite pass. In both applications, passes over the network would be treated as independent. However, in the latter application, since only single passes can be considered, the whole network must be measured at once. Therefore, the forward model must include as many different trajectory offset and drift parameters as independent passes. When these parameters are modeled, the a priori uncertainty in vehicle trajectory can be reduced to 5 cm. A least-squares adjustment method is then used for solving the inverse problem which operates a progressive resolution of common unknowns for each laser-shot. Therefore, a partial Choleski decomposition is implemented. The a posteriori uncertainty is computed from the reduced normal matrix, which is thus merely composed of CCR coordinates, offsets and drifts in vehicle trajectory.

The influence of instrumental and experimental parameters has been analyzed in order to assess the ultimate precision achievable in a specific ground-based experiment. In particular, it has been shown that unresolved vertical coordinates and unknown reference CCR locations essentially produce repetitive distortions in the adjusted coordinates. These can be removed by considering differential solutions. Numerical simulations showed that a beam divergence of 10° limits the precision in transverse and radial coordinates, respectively, to 1.2 cm and 1.1 mm with ~260 measurements per CCR and a single-shot ranging accuracy of 1 cm. There a realistic model was used, which includes offset and drift parameters. Disregarding these parameters produces strong biases in CCR coordinate estimates of up to 6 cm in T and 5 mm in R. It has also been shown that the use of PRs instead of accurate ranges does not have a significant effect on the final positioning accuracy in small networks. This considerably relaxes instrumental constraints, since only that part of the signal containing the echoes need be recorded. This aspect may be particularly important for the development of a spatial instrument.

A specific ground-based experiment of 10^3 laser-shots on a 23-CCR network provided data from which the positioning precision could be assessed. RMS scatters between successive runs of 1.8–3.8 cm and 1–2.3 mm in transverse and radial coordinates, respectively, have been reported. This agrees well with predictions from covariance matrix and numerical simulations.

Hence, two important statements arise. First, the proposed instrument and related signal processing achieve accurate PR measurements without significant biases. In particular, laser biases are both compensated by the adjustment of offsets in vehicle trajectory and reduced owing to the scintillation and/or speckle modulation. However, a further improvement of the present instrument has been undertaken in two directions with the aim of providing a high link budget required for future aircraft experiments. (1) The transimpedance amplifier of the detection stage is optimized on the basis of a minimization of the single-shot ranging accuracy. (2) The use of more sensitive detectors, such as APDs, still of large photosensitive area, is considered. Second, the multilateration problem is properly modeled and efficient procedures for the adjustment and outlier detection have been implemented. However, the latter might still be improved with filtering techniques.

When extrapolating the results of the ground-based experiment to aerial and spatial configurations, 1-mm resolution is expected in relative radial coordinates, given a proper scaling of the instrument. However, many specific aspects of these configurations are still to be studied. For instance, atmospheric effects such as deviations in PD at mesoscale, scintillation, and cloud-cover should be considered. Future numerical simulations should also include a more realistic model for the link budget.

An airborne experiment is planned for 1998 as a second experimental step. Once validated, the technique would thus be a candidate solution for the periodic monitoring of land subsidence such as occurring over gasfields. Another application would be the use of our technique conjointly with static-GPS measurements in large networks. By using GPS stations equipped with CCRs as reference points, our technique would then basically yield a higher density network with an accu-

racy limited by the GPS technique. There, small-scale deformations could be monitored with a typical centimeter accuracy in all three components.

Acknowledgements. The authors would like to acknowledge F. Barlier at the Observatoire de la Cte d'Azur (OCA), Grasse, France, for his support in this work, and F. Pierron and his team of the Ultra-Mobile SLR Station of the OCA, for having contributed to the experiments presented here. They would also like to acknowledge D. Bruneau of the Service d'Aéronomie-CNRS, Paris, France, for his contribution in laser instrumentation, and D. Fourmaintraux of Elf Aquitaine, Pau, France, for his interest in this project.

References

Bar-David I (1969) Communication under the Poisson Regime. IEEE Trans Inf Theory 15: 31–37

Bock O (1996) Study of a wide-angle airborne laser ranging system with ground-based retroreflecting benchmarks for vertical ground deformations monitoring. Study of the adaptation to a spaceborne platform (in French), PhD thesis, University of Paris 7, France

Bock O, Thom C. Kasser M, Fourmaintraux D (1995) Development of a new airborne laser subsidence measurement system, aiming at mm-accuracy. In: Barends FBJ, Brouwer FJJ, Schröder FH (ed) Land Subsidence, Proc 5th Int Symp Land subsidence, The Hague, Balkema, Rotterdam pp 113–122

Bock O, Kasser M, Thom C, Pelon J (1998) Multilateration with the wide-angle laser ranging system: ranging performance and first ground-based validation experiment. IEEE Trans Geosci Remote Sensing: in press

Bouteca MJ, Fourmaintraux D, Meimon Y (1990) In situ measurements and numerical modeling of the reservoir compacting and surface subsidence. In: Imafiso G, Frias M, Bentgen JM (ed), Proc Eur Oil and gas conf, Palermo pp 127–135

Christodoulidis DC, Smith DE, Kolenkiewicz R, Klosko SM, Torrence MH, Dunn PJ (1985) Observing tectonic plate motions and deformations from satellite laser ranging. J Geophys Res 90: 9249–9263

Cohen SC, Degnan JJ, Bufton JL, Garvin JB, Abshire JB (1987) The geoscience laser altimetry/ranging system. IEEE Trans Geosci Remote Sensing 25: 581–592

Davis J, Herring TA, Shapiro I, Rogers A, Elgered G (1985) Geodesy by radio-interferometry: effects of atmospheric modeling errors on estimates of baseline lengths. Radio Sci 20: 1593–1607

Degnan JJ (1985) Satellite laser ranging: current status and future prospectus. IEEE Trans Geosci Remote Sensing 23: 398–413

Degnan JJ (1993) Millimeter accuracy satellite laser ranging: a review. In: Contributions of space geodesy to geodynamics: technology. Geodynamics ser 25, American Geophysical Union, pp 133–162

Dingwen L (1989) Some general problems of the interpretation of geodetic deformation data. In: Vyskocil P, Reigber C, Cross PA (ed) Global and regional geodynamics Proc IAG, Edinburgh. Springer, Berlin Heidelberg New York, pp 369–375

Dodson AH, Shardlow PJ, Hubbard LCM, Elgered G, Jarlemark POJ (1996) Wet tropospheric effects on precise relative GPS height determination. J Geod 70: 188–202

Fourmaintraux D, Flouzat M, Bouteca MJ, Kasser M (1994) Improved subsidence monitoring methods. In: Int Symp SPE-ISRM Eurock'94. Balkema, Rotterdam, pp 549–556

Genrich FJ, Bock Y (1992) Rapid resolution of crustal motion at short ranges with the GPS. J Geophys Res 97: 3261–3269

Glaus R, Bürki B, Kahle HG (1995) Recent results of water vapor radiometry in assessing vertical lithospheric movements by using space geodetic radiowave techniques. J Geodyn 20: 31–39

Goodman JW (1975) Statistical properties of laser speckle patterns. In: Dainty JC (ed) Laser speckle and related phenomena. Springer, Berlin Heidelberg New York, pp 9–75

Gracheva ME, Gurvich AS, Kashkarov SS, Pokasov VV (1978) Similarity relations and their experimental verification for strong intensity fluctuations of laser radiation. In: Strohbehn JW (ed) Laser beam propagation in the atmosphere. Springer, Berlin Heidelberg New York, pp 107–127

Herring TA (1992) Submillimeter horizontal position determination using VLBI. J Geophys Res 97: 1981–1990

Heywood C (1995) Investigation of aquifer-system compaction in the Hueco basin, El Paso, Texas, USA. In: Barends FBJ, Brouwer FJJ, Schröder FH (ed) Land Subsidence IAHS Publication. Proc 5th Int Symp Land subsidence, The Hague, Balkema, 234, pp 35–45

Kahn WD, Vonbun FO, Smith DE, Englar TS, Gibbs BP (1980) Performance analysis of the Spaceborne Laser Ranging System. Bull Geod 54: 165–180

Kahn WD, Degnan JJ, Englar TS (1982) The airborne laser ranging system, its capabilities and applications. Nasa Tech Memo 83984, GSFC, Greenbelt, Md

Kasser M, IGN (1991) Method for determining the spatial coordinates of points, applications of said method to high-precision topography, system and optical device for carrying out said method. US Patent 774038, Eur patent 91402698.4

Lundqvist G (1984) Radio-interferometry as a probe of tectonic plate motion. Tech rep 150, School of Electrical and Computer Engineering, Chalmers University of Technology, Göteborg, Sweden

Lutz H, Krause W, Barthel G (1982) High-precision two-colour spaceborne laser ranging system for monitoring geodynamic processes. In: American Institute of Aeronautics and Astronautics, Inc., 1983, (ed) 33rd Congr Int Astronautical Federation, Paris, France. pp 237–254

Marini JW, Murray CW (1973) Correction of laser range tracking data for atmospheric refraction at elevation above 10 degrees. Nasa Tech Memo, X 591-73-351 GSFC, Greenbelt, Md

Massonnet D, Briole P, Arnaud A (1995) Deflation of Mount Etna monitored by spaceborne radar interferometry. Nature 375: 567–570

Ruegg JC, Kasser M (1990) Deformation across the Asal-Ghoubbet rift, Djibouti. Uplift and crustal extension. Geophys Res Lett 64: 63–72

Santerre R (1991) Impact of GPS satellite sky distribution. Manuscr Geod 16: 28–53

Smith DE, Kolenkiewicz R, Dunn PJ, Robbins JW, Torrence MH, Klosko SM, Williamson RG, Pavlis EC, Douglas NB, Fricke SK (1990) J Geophys Res 95: 22013–22041

Strohbehn JW (1978) Modern theories in the propagation of optical waves in a turbulent medium. In: Strohbehn JW (ed) Laser beam propagation in the atmosphere. Springer, Berlin Heidelberg New York, pp 45–106

Tapley BD, Schultz BE, Eanes RJ (1985) Station coordinates, baselines, and earth rotation from lageos laser ranging: 1976–1984. J Geophys Res 90: 9235–9248

Tarantola A (1987) Inverse problem theory, methods for data fitting and model parameters estimation. Elsevier, Amsterdam

Willis P (1996) Le système Doris: applications actuelles à l'IGN et perspectives d'avenir. Journées Recherche, IGN Saint Mandé, France

Ware R, Rocken C, Solheim F, Van Hove T, Alber C, Johnson J (1993) Pointed water vapor radiometer correction for accurate GPS surveying. Geophys Res Lett 20, 2635–2638